engineering proceedings

MDPI

Proceeding Paper

Towards Predictive Models of Mechanical Properties in 3D-Printed Polymers: An Exploratory Study †

Bruno A. G. Sousa [1,2,*], César M. A. Vasques [1,2,*] and Adélio M. S. Cavadas [1]

[1] proMetheus, Higher School of Technology and Management, Polytechnic Institute of Viana do Castelo (IPVC), 4900-347 Viana do Castelo, Portugal; adelioc@estg.ipvc.pt
[2] Centre for Mechanical Technology and Automation (TEMA), Department of Mechanical Engineering, Universidade de Aveiro, 3810-193 Aveiro, Portugal
* Correspondence: b.sousa@ipvc.pt (B.A.G.S.); cmavasques@ua.pt (C.M.A.V.)
† Presented at the 6th International Electronic Conference on Applied Sciences, 9–11 December 2025; Available online: https://sciforum.net/event/ASEC2025.

Abstract

Additive manufacturing, particularly 3D printing, is increasingly shaping the production of polymer-based components, enabling complex geometries and tailored functional performance. Yet, predicting their mechanical behavior remains challenging due to material anisotropy and sensitivity to processing conditions. This work presents an exploratory study designed to provide the experimental basis for the development and calibration of predictive models of mechanical properties in 3D-printed components. Standard ISO 527-2 Type 1A specimens were fabricated using thermoplastic PLA (polylactic acid) with systematic variations in layer orientation, infill overlap, and printing velocity. Mechanical characterization was carried out through uniaxial tensile testing to determine tensile strength and stiffness of the material specimens, while scanning electron microscopy (SEM) provided complementary insights into interlayer bonding, filament alignment, porosity, and fracture morphology. Results showed that material type and processing strategies strongly influenced mechanical response, with SEM highlighting microstructural features that govern interlayer adhesion and failure mechanisms. These findings contribute to a deeper understanding of process–structure–property relationships in additive manufacturing and establish the groundwork for predictive model development. Ongoing efforts will integrate these experimental insights into numerical simulations employing homogenized material models, thereby enhancing design optimization and reliability of 3D-printed structural components.

Keywords: additive manufacturing; polymers; material extrusion; process–structure–property relationship; mechanical characterization

Check for updates

Academic Editor: Ana Martins Amaro

Published: 16 March 2026

Copyright: © 2026 by the authors. Licensee MDPI, Basel, Switzerland. This article is an open access article distributed under the terms and conditions of the Creative Commons Attribution (CC BY) license.

1. Introduction

Material extrusion (MEX) additive manufacturing, often referred to as fused filament fabrication (FFF) or fused deposition modeling (FDM), is now widely used to produce polymer components with complex geometries and tailored functions, although the mechanical reliability of printed parts frequently trails bulk materials because of anisotropy, voids, and microstructures that depend strongly on the process [1–3]. Unlike subtractive manufacturing, MEX constructs parts in discrete beads and layers, which introduces directional interfaces, steep thermal gradients, and incomplete polymer diffusion that together produce direction-dependent stiffness, strength, and failure mechanisms [4–6]. For widely

used thermoplastics, such as polylactic acid (PLA) and acrylonitrile butadiene styrene (ABS), these effects create pronounced sensitivity to build orientation, raster angle, and deposition speed, which makes predictive design difficult without carefully controlled experiments and material characterization [7–9].

Interlayer adhesion is a central barrier in MEX because it is governed by transient thermal histories and chain diffusion across interfaces, and it often limits Z-axis properties while promoting delamination; recent studies demonstrate that both toolpath strategies and process-adjacent treatments can reduce voids and improve bonding [10–12]. Microstructural defects, particularly voids that arise between tracks and layers, correlate strongly with tensile strength reductions and brittle fracture paths, which motivates scanning electron microscopy and image analysis to quantify porosity and link it to macroscopic response at the mesoscale [13,14]. In parallel, homogenization frameworks and anisotropic constitutive descriptions are increasingly used to translate MEX mesostructure, including void shape and size, bead overlap, and coalescence areas, into effective stiffness and strength tensors for finite element simulations [15–17].

The present exploratory study uses ISO 527-2 [18] Type 1A tensile specimens fabricated in PLA and varies layer orientation, infill overlap, and printing velocity to build an experimental basis for calibrating predictive models of mechanical properties, in close agreement with evidence that build orientation and raster geometry dominate tensile response while speed and temperature produce second-order effects within practical ranges [7,9]. Uniaxial tensile testing provides tensile strength and stiffness, and scanning electron microscopy reveals interlayer neck growth, filament alignment, porosity, and fracture morphology, all of which repeatedly govern failure in neat polymers and reinforced systems [6,19]. The combination of standardized mechanical characterization and microstructural imaging is essential to disambiguate processing effects and to inform model parameterization, particularly when anisotropy is driven by bead-level architecture rather than intrinsic resin behavior [2,4,5].

Systematic investigations confirm that raster angle and orientation critically control tensile and flexural properties, with 0° to 0° aligned rasters usually maximizing unidirectional strength, while ±45° configurations promote increased ductility and/or interlaminar failure and reduce ultimate strength, which is consistent with anisotropic stress transfer across bead interfaces [20,21]. For PLA, orientation-induced variability can exceed 40% to 50% in tensile strength, which underscores the need to capture orientation as an explicit descriptor in experimental design and in subsequent modeling frameworks [7–9]. Printing speed and nozzle temperature influence melt rheology and neck formation, and data show non-monotonic trends across materials; PLA may benefit from moderately higher temperatures that enhance interdiffusion [3]. Due to the sensitivity and impact of all these process parameters, there is a need to conduct standardized experimental studies, both at the process level and at the material characterization level, such as those used in this study, in order to identify and isolate the key parameters that have the greatest impact on mechanical performance and thereby develop a reproducible experimental methodology [1,4].

From a microstructural perspective, void topology and interlaminar bonding remain recurrent determinants of strength and fracture, and both can be quantified through SEM and image analysis to parameterize meso-scale representative volume elements for homogenization and damage modeling [14,15,22]. Process-level strategies, such as interlaced deposition [0°/90°], as well as deposition at different raster angles and filament chemical treatments, show measurable reductions in porosity and increases in interlaminar shear strength, which provide mechanistic levers that can be encoded into process–structure–material maps for predictive simulation [10–12]. These advances complement data-driven approaches in which machine learning (ML) regressors and neural

networks predict mechanical properties from process parameters, thereby enabling rapid design iteration and feature importance analyses that highlight key drivers such as layer thickness and bed temperature [22,23]. Although many ML studies focus on metals or composites, the methodological principles that involve multioutput regression, model explainability, and transfer learning are directly portable to polymer MEX and can augment physics-based models with statistically grounded parameter sensitivities [11,12,22].

Accordingly, the literature identifies the main challenges of the MEX process, which include a dominant influence of build orientation on tensile behavior, limited effects of speed and temperature within practical ranges, and a critical role for interlayer adhesion and voids. These challenges are therefore consistent with current research and motivate the integration of homogenized material laws into numerical simulations to improve design reliability [7,9,15]. The combination of experimental data on tensile strength, stiffness and fracture morphology with constitutive frameworks calibrated to orientation and raster sequences can reproduce stress–strain behavior up to the onset of damage and enable optimization against microstructural constraints [2,4,17]. In parallel, homogenization that incorporates measured void content and coalescence areas supports virtual testing of deposition strategies and can reduce physical iteration, guiding process windows for PLA components [3,10,15].

In summary, this work addresses the process–structure–property nexus in polymer extrusion additive manufacturing (MEX) through a disciplined experimental program on PLA tensile specimens, complemented by SEM, thereby establishing the evidence base required to develop predictive models [1,5,24]. By leveraging these insights, subsequent numerical simulations and data-driven tools can enhance design optimization and structural reliability of 3D-printed components [4,11,17].

2. Materials and Methods

2.1. CAD Design and Microstructural Prediction

Firstly, a geometric study was conducted to predict internal morphology resulting from the unidirectional deposition strategy. A CAD model of the cross-section of the specimen to be subsequently printed was generated to simulate the arrangement of adjacent extruded filaments and to estimate the presence of voids between layers and between filaments. Figure 1 shows the CAD deposition prediction of the cross-section of the specimen. For a linear deposition strategy with only a small overlap between filaments due to the heat generated, Figure 1a shows a higher number of voids. However, considering the pressure exerted by the nozzle and the thermal effects between filaments, it is possible that two adjacent filaments exhibit a stronger bond, resulting in an enlarged fusion zone (Figure 1b).

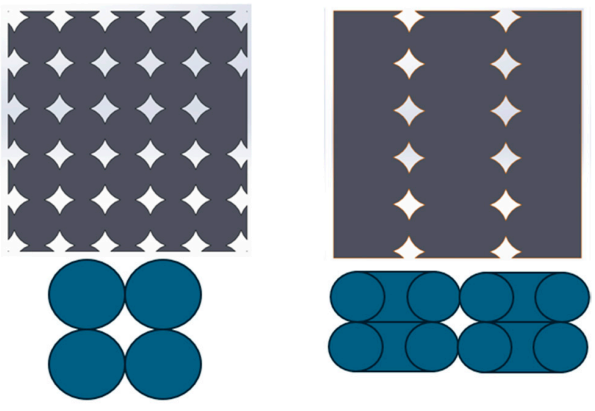

(**a**) (**b**)

Figure 1. Deposition prediction: Linear approach (**a**); strong bond between filaments (**b**).

As this type of approach is common in MEX research to anticipate mesostructural features arising from the discrete nature of filament deposition, it was possible to identify that these voids are consistent with the triangular or lens-shaped gaps frequently reported in the literature for unidirectional deposition patterns. In such patterns, the filament cross-section deviates from an ideal circular or rectangular geometry due to the combined effects of extrusion pressure, nozzle geometry, and layer height [20,25,26].

To validate the predictions obtained from the CAD model, a scanning electron microscopy (Hitachi SU1510, Hitachi High-Tech, Tokyo, Japan) analysis (SEM) was performed on the fractured cross-sections of the printed specimens. SEM is widely used to characterize the mesostructure of MEX materials, enabling the assessment of inter-filament bonding quality, void morphology, and potential defects that are not readily observable using optical methods [27].

According to the literature, the properties of PLA can vary depending on the filament manufacturing process. Table 1 shows the range of properties:

Table 1. PLA properties based on the literature [28,29].

Properties	Seas3d.com [28]	JuggerBot3D [29]
Stiffness [MPa]	3500	4200
Tensile Strength [MPa]	26–60	38–48
Density [g/cm^3]	1.24–1.30	1.08–2.12

2.2. Materials, Printing and Specimen Preparation

Commercial PLA filaments were selected due to their widespread use in MEX and the extensive literature on process–structure–property relationships [3–5]. The filaments were stored in sealed containers with desiccant for at least 48 h before printing to mitigate moisture-related defects [5,13]. As shown in Figure 2, the specimens were produced on a Creality Ender-3 V2 printer (Shenzhen Creality 3D Technology Co., Ltd., Shenzhen, China), a Cartesian bed-slinger, nominal build volume 220 × 220 × 250 mm, which supports hot-end temperatures up to ~260 °C and bed temperatures up to ~100 °C, suitable for PLA [30,31]. Slicing was performed in Cura with a 0.4 mm nozzle, 0.2 mm layer height, and 100% flow, unless otherwise stated; the PLA range temperatures were 200–220 °C for the nozzle and 60 °C for the bed, with part cooling enabled for PLA to promote interlayer fusion [30,32].

A controlled parametric matrix was designed to quantify the effects of build orientation (flat XY, on-edge XZ, upright YZ), deposition temperature (baseline and +10%), and printing speed (12.5, 25, 50 mm/s). Regarding the orientation of planes, material deposition followed the XY plane for both contour and unidirectional raster deposition. All specimens were manufactured in this plane, while the deposition of subsequent layers occurred along either the XZ or YZ plane, which defines the specimen thickness.

Factor levels were selected within ranges commonly reported for FFF polymers, where orientation and raster geometry dominate tensile response, while speed and temperature provide secondary influences [3,6,7,9,19,32]. Tensile specimens followed ISO 527-2 prescriptions for rigid/semi-rigid plastics using the Type 1A/A1 dog-bone geometry recommended for inter-laboratory comparability; specimens were printed unidirectionally and 100% rectilinear infill without post-processing to avoid confounding effects [33]. Table 2 presents the process parameters, with a focus on the main variations between the baseline and the defined case studies. Figure 3 shows an illustration of the material deposition orientation: (a) unidirectional contour orientation and (b) unidirectional line orientation.

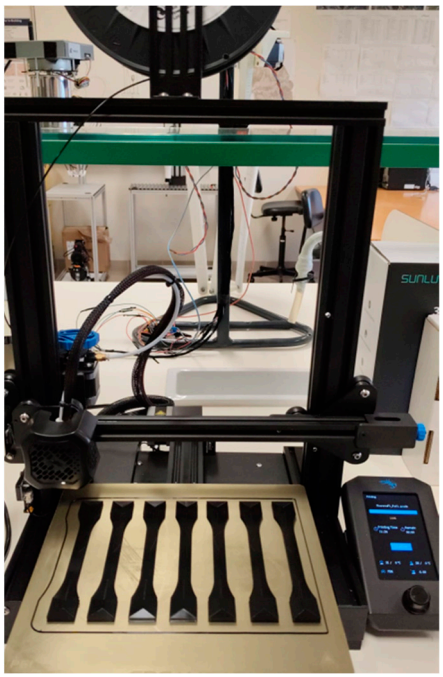

Figure 2. 3D-printer Creality Ender-3 V2 and specimens.

Table 2. Process parameter definitions (baseline vs. case studies).

Parameters	Baseline	Case Study 1	Case Study 2	Case Study 3	Case Study 4
Nozzle temp. (°C)	200	200	200	220	200
Bed temp. (°C)	60	60	60	60	60
Print speed (mm/min)	25	50	12.5	25	25
Deposition orientation	Figure 3a				Figure 3b

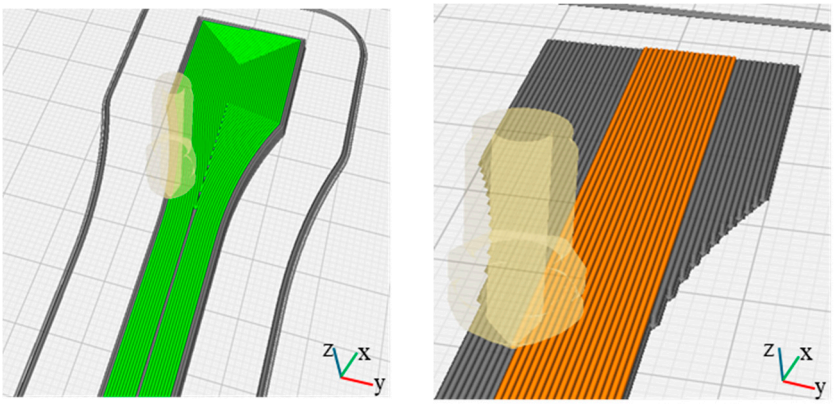

(**a**) (**b**)

Figure 3. Scheme of deposition orientation: (**a**) unidirectional contour orientation; (**b**) unidirectional line orientation.

The specimens for SEM analysis were prepared as follows: The specimens were cut through the central section, with a maximum dimension of approximately 3 cm; they were embedded in a two-component epoxy resin (resin and hardener). Once the mixture was prepared, the specimens were submerged in the resin and left to cure for approximately 48 h. After the resin block containing the specimen was obtained, the samples were subjected to a polishing process. This began with coarser abrasive paper to remove any residues on the surface and to level the section, followed by sequentially finer grits. The grit sequence used was 400/600/800/1200.

2.3. Characterization and Testing

The samples subjected to physical and mechanical characterization were weighed using a balance with an accuracy of 0.1 mg, and the dimensions of the gauge section were measured using a caliper with an accuracy of 0.01 mm.

The apparent density was determined in accordance with ASTM D792 [34] by weighing the samples in air and subsequently while immersed in water. Based on Archimedes' principle, the apparent density was then calculated; in this way, the apparent density served as an indicator of differences in sample porosity among the sets of process parameters under study [8,15,33].

The surface texture was evaluated using two methods: The first employed a Mitutoyo SJ-210 (Mitutoyo SJ-210, Mitutoyo Corporation, Kawasaki, Kanagawa, Japan) surface roughness tester in accordance with ISO 4287:1997 [35] and analyzed over the gauge length (50 mm) at three positions: the center, and 25 mm above and below this point. The second used a scanning electron microscope (SEM). For the two, Ra, Rq and Rz were analyzed to capture the surface trend and how this has an impact on the mechanical performance of the specimens [18,36].

Uniaxial tensile tests were performed on a Shimadzu AGX-100 kN (Shimadzu AGX-100kN, Shimadzu Corporation, Kyoto, Japan) frame equipped with a high-precision load cell of 100 kN and a video extensometer. The tests followed ISO 527-2 with a preferred 50 mm gauge length, a speed rate of 1 mm/min. and a data acquisition of 10 Hz to determine the tensile strength and stiffness [33,37]. Primary outcomes were stiffness and tensile strength, which are essential properties for thermoplastic materials and for evaluating anisotropy in MEX parts [3,33]. Fracture surfaces and polished cross-sections were examined by SEM to evaluate the interlayer bonding and void morphology.

2.4. Data Reduction and Statistics

Stress–strain curves were computed from the recorded force and extensometer strain. The tensile modulus was obtained by linear regression of the initial elastic segment, tensile strength at the maximum stress, and elongation at break at specimen separation, following ISO 527-2 reporting [33]. Results are presented as mean ± standard deviation and are compared based on the process parameters altered relative to the baseline, to identify the individual impact of each parameter.

3. Results

3.1. Property Prediction Based on Deposition CAD Design

The CAD analysis revealed an estimated void volume fraction of approximately 18% for the linear deposition approach and 6% for the case in which enhanced bonding between filaments is present. These voids are predominantly located in the regions between adjacent extruded lines. The voids are consistent with the triangular or lens-shaped gaps frequently described in the literature for unidirectional deposition patterns, in which the filament cross-section deviates from an ideal circular or rectangular geometry due to the combined effects of extrusion pressure, nozzle geometry, and layer height.

Given the presence of these voids, it is evident that they influence the mechanical performance of MEX components by acting as stress concentrators and reducing the effective load-bearing area, as highlighted by several authors studying the microstructural origins of anisotropy in PLA parts.

Considering that the stiffness reported for this material ranges between 3500 MPa and 4200 MPa, and considering the 6% void fraction, the stiffness could decrease to values between 3290 MPa and 3948 MPa, based solely on the voids formed due to the deposition orientation.

3.2. Printing Fidelity, Density and Surface Condition

All test samples were produced without critical defects, such as layer misalignment during printing or significant dimensional non-conformities, and seven samples were produced for each condition. The density was determined by first measuring the mass of each sample in air and then submerging each sample in water (since PLA has a density higher than water) to obtain the immersed mass. Following the standard ASTM D792, the density was calculated based on Archimedes' principle

$$\rho_s = \frac{A}{A - B} \cdot (\rho_w - \rho_a) \cdot \rho_a \quad (1)$$

where ρ_s is the density of the specimen, A is the mass of the specimen in air, B is the mass of the specimen submerged in water, ρ_w is the density of water at 20 °C and ρ_a is the density of air at 20 °C.

Figure 4 shows the mean mass for each condition (a) and the corresponding density for each condition (b).

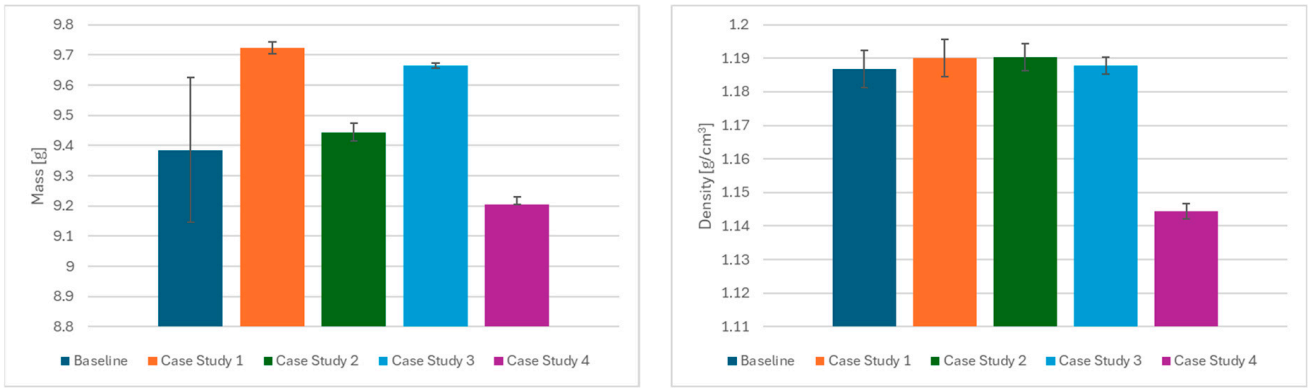

(**a**) (**b**)

Figure 4. Physics results: mass results (**a**); density results (**b**).

Based on this analysis, the roughness tester provided a surface profile of each sample, and the main parameter values were recorded; Figure 5 presents the results for each parameter (in microns) for all conditions under study.

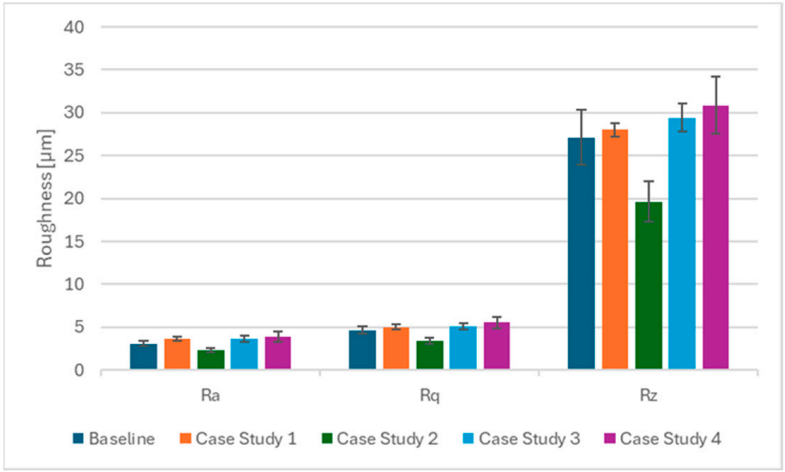

Figure 5. Roughness results for all studies (Ra, Rq and Rz).

3.3. Tensile Behavior

In accordance with ISO 527-2, the main mechanical properties were obtained for each test condition, namely, stiffness, which indicates sample stiffness, and tensile strength, which indicates resistance. Based on the obtained results, the mean value for each study was calculated, along with the associated standard deviation for each property.

Table 3 summarizes the results, presenting the mean values and standard deviations for each study condition.

Table 3. Summary of tensile test results.

Parameters	Young Modulus [MPa]	Maximum Strength [MPa]
Baseline	3944.7 ± 361	53.8 ± 0.7
Case Study 1	3548.9 ± 284	55.9 ± 1.5
Case Study 2	3605.2 ± 122	51.5 ± 1.4
Case Study 3	3440.3 ± 174	53.6 ± 0.6
Case Study 4	3345.5 ± 228	37.2 ± 12.5

The tensile results are presented in Figure 6, with a focus on the stiffness and maximum stress between the baseline and the defined case studies.

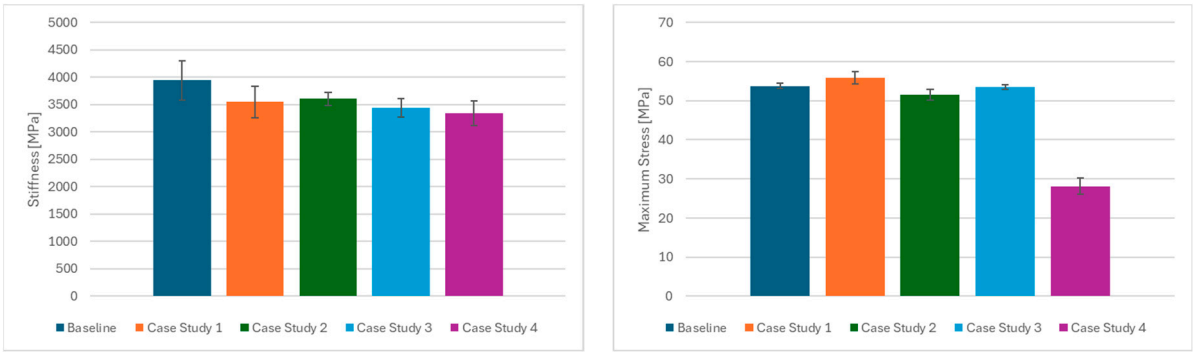

(**a**) (**b**)

Figure 6. Tensile test results comparing baseline vs. case studies: Stiffness (**a**); maximum stress (**b**).

3.4. SEM Analysis

Figure 7 shows the specimen after polishing. Subsequently, it was subjected to a carbon coating treatment to enhance the imaging quality produced by the electron beam (the operating principle of SEM).

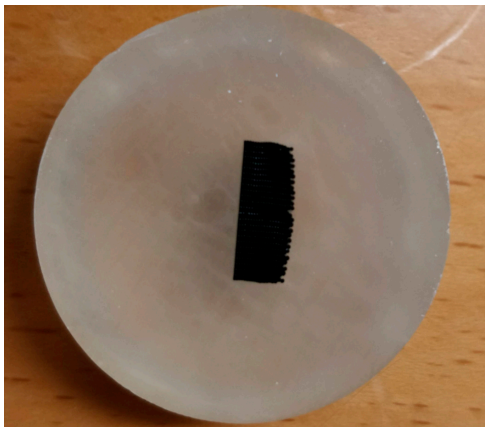

Figure 7. Specimen preparation for SEM analysis.

Based on the SEM analysis, it can be observed in Figure 8 that the voids in the specimen correspond in location and exhibit a shape identical to that predicted by the CAD model. Thus, it is possible to determine the cross-section of MEX-manufactured parts, and, in the case of a unidirectional section, the void shape and position are more uniform.

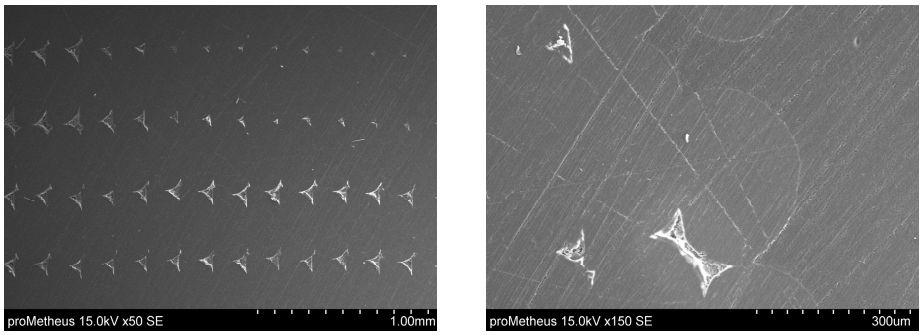

(**a**) (**b**)

Figure 8. Cross-section of a baseline sample on SEM, existence of voids between filaments: 50× zoom (**a**); 150× zoom (**b**).

4. Discussion

For a better understanding of the results analysis, the variation in the process parameters between the baseline and the remaining cases studied is again presented, as shown in Table 2.

Considering the variations in process parameters, with respect to porosity analysis based on mass and density measurements, no significant fluctuations were observed. The largest variations were approximately 3% in mass (between the baseline and Case Study 1) and approximately 2% in density (between the baseline and Case Study 4).

For surface roughness, the parameters Ra, Rq, and Rz showed more pronounced variations between the baseline and Case Study 2, with differences of approximately 26%, 28%, and 27%, respectively. Case Study 2 exhibited lower Ra, Rq, and Rz values, indicating that a lower printing speed results in higher precision and reduced filament deposition variability. The remaining case studies showed similar surface roughness parameter values.

Based on the predictive parameters considering only the unidirectional deposition orientation, the existing voids lead to a reduction in stiffness of approximately 6%, resulting in a stiffness range between 3290 and 3948 MPa. Observing the experimental results, all cases studied exhibit stiffness values within this range.

In the experimental tests, although the stiffness values were generally similar across different conditions, the baseline showed the highest stiffness of 3.9 GPa. Conversely, Case Study 4 presented the lowest stiffness and tensile strength among all sets (3.3 GPa and 37 MPa), indicating that filament deposition orientation is the parameter with the greatest impact on the mechanical performance of 3D-printed parts. This variation is associated with discontinuous deposition (as in unidirectional line deposition), which can generate residual stresses due to material discontinuity and poor adhesion between successive filaments. In contrast, contour deposition maintains a more uniform line, promoting better interlayer adhesion.

Regarding SEM analysis, filament deposition patterns and their interactions, as well as micro-voids between filaments, were observed, consistent with expectations for this type of deposition. Nevertheless, further work is needed to improve the correlation between deposition patterns, geometric trends, and mechanical performance results.

https://doi.org/10.3390/engproc2026124079

5. Conclusions

In the investigation of the influence of process parameters on the mechanical performance of 3D-printed parts, studies were conducted on porosity generated during the process, surface roughness, and stiffness/strength analysis in relation to process variations. The following conclusions can be drawn from the investigation:

- Manufacturing orientation predominantly affects tensile behavior, outweighing the effects of printing speed and temperature within practical ranges. Discontinuous deposition (as in unidirectional line deposition) can generate residual stress due to material discontinuity and poor adhesion between successive filaments, whereas contour depositions maintain a more uniform line, promoting better interlayer adhesion.
- Printing speed and temperature influence surface finish and dimensional accuracy but have minimal impact on mechanical strength. However, the results indicate that higher printing speeds lead to greater strength, while higher temperatures produce the opposite effect. This can be attributed to the fact that higher printing speeds reduce the cooling time between successive layers, thereby minimizing residual stress generated by material shrinkage and improving localized defects that lead to fracture. However, increasing the temperature results in a larger thermal shock to the material, which reduces crystallization and consequently decreases stiffness; this can also lead to a reduction in strength.
- Mass and density studies show that existing variations do not have a significant impact, similar to the surface roughness analysis.
- SEM analysis allowed observation of filament deposition patterns and their interactions, as well as the micro-voids between filaments. Nonetheless, this technique could be further explored to establish a better correlation between deposition patterns and mechanical performance.

Author Contributions: Conceptualization, B.A.G.S., C.M.A.V. and A.M.S.C.; methodology, B.A.G.S., C.M.A.V. and A.M.S.C.; software, B.A.G.S.; validation, B.A.G.S., C.M.A.V. and A.M.S.C.; formal analysis, B.A.G.S., C.M.A.V. and A.M.S.C.; investigation, B.A.G.S., C.M.A.V. and A.M.S.C.; resources, C.M.A.V. and A.M.S.C.; data curation, B.A.G.S.; writing—original draft preparation, B.A.G.S.; writing—review and editing, B.A.G.S., C.M.A.V. and A.M.S.C.; funding acquisition, C.M.A.V. and A.M.S.C. All authors have read and agreed to the published version of the manuscript.

Funding: The authors gratefully acknowledge the funding provided by the Foundation for Science and Technology (FCT) of Portugal, within the scope of the project of the Research Unit on Materials, Energy and Environment for Sustainability (proMetheus, https://tech.ipvc.pt/unidades.php?u=PROMETHEUS (accessed on 24 January 2026)), Ref. UID/05975/2020, financed by national funds through the FCT/MCTES, and the funding provided within the scope of the "Agenda DRIVOLUTION: Transition to the Factory of the Future", project no. C632394276-0046698 with operation code 02/C05-i01.02/2022.PC644913740-00000022, within the framework of the Agendas/Mobilizing Alliances for Reindustrialization, Notice no. 2022-C05i0101-02, project 23, of the Recovery and Resilience Plan (PRR) of Portugal.

Institutional Review Board Statement: Not applicable.

Informed Consent Statement: Not applicable.

Data Availability Statement: Data are contained within the article.

Conflicts of Interest: The authors declare no conflicts of interest.

References

1. Sing, S.L.; Yeong, W.Y. Process–Structure–Properties in Polymer Additive Manufacturing. *Polymers* **2021**, *13*, 1098. [CrossRef] [PubMed]
2. Bandinelli, F.; Scapin, M.; Peroni, L. Effects of Anisotropy and Infill Pattern on Compression Properties of 3D Printed CFRP: Mechanical Analysis and Elasto-Plastic Finite Element Modelling. *Rapid Prototyp. J.* **2024**, *30*, 142–158. [CrossRef]
3. Menargues, S.; Navas, J.; Espinosa, I.; Baile, M.T.; Vaz, R.F.; Picas, J.A. Effect of Additive Manufacturing Parameters on PLA, ABS, and PETG Strength. *Processes* **2025**, *13*, 2733. [CrossRef]
4. Umer, M.H.; Khan, M.B.; Zafar, M.Q.; Hussain, G.; Ashfaq, B.; Arshad, M.U.; Lughmani, W.A. Influence of Process Parameters on Mechanical Properties and Surface Roughness in Fused Filament Fabrication: A Comprehensive Review. *J. Braz. Soc. Mech. Sci. Eng.* **2025**, *47*, 259. [CrossRef]
5. Cojocaru, V.; Frunzaverde, D.; Miclosina, C.-O.; Marginean, G. The Influence of the Process Parameters on the Mechanical Properties of PLA Specimens Produced by Fused Filament Fabrication—A Review. *Polymers* **2022**, *14*, 886. [CrossRef]
6. Qayyum, H.; Hussain, G.; Sulaiman, M.; Hassan, M.; Ali, A.; Muhammad, R.; Wei, H.; Shehbaz, T.; Aamir, M.; Altaf, K. Effect of Raster Angle and Infill Pattern on the In-Plane and Edgewise Flexural Properties of Fused Filament Fabricated Acrylonitrile–Butadiene–Styrene. *Appl. Sci.* **2022**, *12*, 12690. [CrossRef]
7. Syaefudin, E.A.; Kholil, A.; Hakim, M.; Wulandari, D.A.; Riyadi; Murtinugraha, E. The Effect of Orientation on Tensile Strength 3D Printing with ABS and PLA Materials. *J. Phys. Conf. Ser.* **2023**, *2596*, 012002. [CrossRef]
8. dos Santos, N.V.; Cavalcanti, D.K.K.; Neto, J.S.S.; de Queiroz, H.F.M.; Banea, M.D.; Cardoso, D.C.T. Analysis of Voids, Interfacial and Thermal Properties of Additively Manufactured Continuous Natural Fiber-Reinforced Biocomposites. *Prog. Addit. Manuf.* **2025**, *10*, 5401–5422. [CrossRef]
9. Eryildiz, M. Effect of Build Orientation on Mechanical Behaviour and Build Time of FDM 3D-Printed PLA Parts: An Experimental Investigation. *Eur. Mech. Sci.* **2021**, *5*, 116–120. [CrossRef]
10. Sun, X.; Mazur, M.; Cheng, C.-T. An Interlaced Toolpath Strategy for Void Reduction in Material Extrusion Additive Manufacturing. *Prog. Addit. Manuf.* **2025**, *10*, 4239–4255. [CrossRef]
11. Fetecau, C.; Stan, F.; Boazu, D. Artificial Neural Network Modeling of Mechanical Properties of 3D-Printed Polyamide 12 and Its Fiber-Reinforced Composites. *Polymers* **2025**, *17*, 677. [CrossRef]
12. Trimini, V.; Stano, G.; Varetti, S.; Corvaglia, S.; Kumar, A.; Percoco, G. Atmospheric Plasma Enhances Interlayer Adhesion in High-Performance 3D-Printed Polymers by Modifying Surface Energy, Morphology and Chemical Composition. *Prog. Addit. Manuf.* **2025**, *10*, 9569–9583. [CrossRef]
13. Alkunte, S.; Gupta, M.; Shingare, K.; More, N.; Mali, A.; Ingle, N.; Nalawade, S.; Khan, A.U.; Sinha, N.; Liao, K.; et al. Porosity in Additive Manufacturing: Influence on Mechanical, Thermal, and Electrical Properties—A Review. *Int. J. Adv. Manuf. Technol.* **2025**, *140*, 2397–2421. [CrossRef]
14. Zhang, S.-U. Numerical Evaluation of ABS Parts Fabricated by Fused Deposition Modeling and Vapor Smoothing. *Adv. Sci. Technol. Eng. Syst.* **2017**, *2*, 157–161. [CrossRef]
15. Springmann, M.; Middendorf, P. Mesoscopic Homogenization Method of Mechanical Properties of Fused Filament Fabrication Structures Considering Void Shapes and Filament Interfaces. *Prog. Addit. Manuf.* **2025**, *10*, 1755–1762. [CrossRef]
16. Ferrano, F.; Fateri, M.; Merkel, M.; Hertel, J. Simulating Elastoplastic and Anisotropic Behavior in Thermoplastic Additively Manufactured Components: An Application-Oriented Modeling Approach. *Polymers* **2024**, *16*, 1234. [CrossRef]
17. Villegas, A.I.; Garcia, J.P.; Carillo, J.; Espalin, D. *Bead-Weaved Layered Prints for Improved Interlayer Adhesion in Additive Manufacturing*; University of Texas at Austin: Austin, TX, USA, 2024.
18. *ISO 527-2:2012*; Plastics—Determination of Tensile Properties—Part 2: Test Conditions for Moulding and Extrusion Plastics. ISO: Geneva, Switzerland, 2012.
19. Çakan, B.G. Effects of Raster Angle on Tensile and Surface Roughness Properties of Various FDM Filaments. *J. Mech. Sci. Technol.* **2021**, *35*, 3347–3353. [CrossRef]
20. Ramírez-Prieto, J.S.; Martínez-Yáñez, J.S.; González-Hernández, A.G. Effect of Raster Angle on the Tensile and Flexural Strength of 3D Printed PLA+ Parts. *AIMS Mater. Sci.* **2025**, *12*, 363–379. [CrossRef]
21. Dewangan, K.; Prabhu, T.R.; Gangi Setti, S. Predicting Mechanical Properties of Polymers in Additive Manufacturing: A Machine Learning Multioutput Regression Approach. *J. Inst. Eng. India Ser. D* **2025**. [CrossRef]
22. Hu, Z.; Yan, W. Data-Driven Modeling of Process-Structure-Property Relationships in Metal Additive Manufacturing. *npj Adv. Manuf.* **2024**, *1*, 3. [CrossRef]
23. Chandra A, N.; Bogu, V.P.; Jatavallabhula, J.K.; Gundeti, S.R.; Pappula, B.; Makgato, S. Machine Learning-Driven Prognosis of Tensile Strength in FDM Printed PLA at Various Raster Angles. *Int. J. Adv. Manuf. Technol.* **2026**, *142*, 1445–1465. [CrossRef]
24. Debreceni, A.; Buri, Z.; Bodzás, S. Linking Process Parameters, Structure, and Properties in Material Extrusion Additive Manufacturing of Polymers and Composites: A Review. *J. Manuf. Mater. Process.* **2025**, *9*, 286. [CrossRef]

25. Ahn, S.; Montero, M.; Odell, D.; Roundy, S.; Wright, P.K. Anisotropic Material Properties of Fused Deposition Modeling ABS. *Rapid Prototyp. J.* **2002**, *8*, 248–257. [CrossRef]
26. Sun, Q.; Rizvi, G.M.; Bellehumeur, C.T.; Gu, P. *Experimental Study of the Cooling Characteristics of Polymer Filaments in FDM and Impact on the Mesostructures and Properties of Prototypes*; University of Texas at Austin: Austin, TX, USA, 2003.
27. Cao, M.; Cui, T.; Yue, Y.; Li, C.; Guo, X.; Jia, X.; Wang, B. Preparation and Characterization for the Thermal Stability and Mechanical Property of PLA and PLA/CF Samples Built by FFF Approach. *Materials* **2023**, *16*, 5023. [CrossRef]
28. Available online: https://www.seas3d.com/MaterialTDS-PLA.pdf (accessed on 24 January 2026).
29. Polylactic Acid (PLA) Filament Review. JuggerBot 3D. Available online: https://juggerbot3d.com/pla-filament-review/ (accessed on 24 January 2026).
30. Ender 3 Filament Guide: Best Settings for PLA, ABS & Co.—The 3D Printer Bee. Available online: https://the3dprinterbee.com/ender-3-filament-guide-settings/ (accessed on 24 January 2026).
31. Staff, E. Creality Ender-3 V2: Everything You Need to Know—PrintaGuide. Available online: https://printaguide.com/creality-ender-3-v2-everything-you-need-to-know/ (accessed on 24 January 2026).
32. Spoerk, M.; Gonzalez-Gutierrez, J.; Sapkota, J.; Schuschnigg, S.; Holzer, C. Effect of the Printing Bed Temperature on the Adhesion of Parts Produced by Fused Filament Fabrication. *Plast. Rubber Compos.* **2018**, *47*, 17–24. [CrossRef]
33. ISO 527-2 | Instron. Available online: https://www.instron.com/en/testing-solutions/iso-standards/iso-527-2/ (accessed on 24 January 2026).
34. *ASTM D792-20*; Standard Test Methods of Density and Specific Gravity (Relative Density) of Plastics by Displacement. ASTM International: West Conshohocken, PA, USA, 2020.
35. *ISO 4287:1997*; Geometrical Product Specifications (GPS)—Surface Texture: Profile Method—Terms, Definitions and Surface Texture Parameters. ISO: Geneva, Switzerland, 1997.
36. Available online: https://cdn.standards.iteh.ai/samples/10132/ae4786c47a6045528cfaef0b28d989b7/ISO-4287-1997.pdf (accessed on 24 January 2026).
37. Available online: https://www.shimadzu.com/an/sites/shimadzu.com.an/files/pim/pim_document_file/brochures/17011/c224-e122.pdf (accessed on 24 January 2026).

Disclaimer/Publisher's Note: The statements, opinions and data contained in all publications are solely those of the individual author(s) and contributor(s) and not of MDPI and/or the editor(s). MDPI and/or the editor(s) disclaim responsibility for any injury to people or property resulting from any ideas, methods, instructions or products referred to in the content.